ARTICLE

Direct MYD88^{L265P} gene detection for diffuse large B-cell lymphoma (DLBCL) *via* a miniaturised CRISPR/dCas9-based sensing chip

Received 00th January 20xx,
Accepted 00th January 20xx

DOI: 10.1039/x0xx00000x

Weihan Sun, † [ab] Wei Guo, †[d] Zhiyi Liu, [b] Sennan Qiao, [b] Ziming Wang, [a] Jiayu Wang, [b] Lingxuan Qu, [b] Liang Shan, [a] Fei Sun, *[ab] Shuping Xu, *[c] Ou Bai *[d] and Chongyang Liang *[ab]

Traditional methods for single-nucleotide variants based on the amplification and the fluorescent signals require expensive reagents and cumbersome instruments, and they are time-consuming for each trial. Here, a porous anodised aluminium (PAA)-based sensing chip modified by deactivated Cas9 (dCas9) proteins and synthetic guide RNA (sgRNA) as the biorecognition receptor is developed, which can be used for the label-free sensing of the diffuse large B-cell lymphoma (DLBCL) MYD88^{L265P} gene by integrating with electrochemical ionic current rectification (ICR) measurement. The sgRNA that can specifically identify and capture the MYD88^{L265P} gene was screened, which has been proved to be workable to activate dCas9 for the target MYD88^{L265P}. In the sensing process, the dCas9 proteins can capture the genome sequence, thus bringing negative charges over the PAA chip and correspondingly resulting in a variation on the ICR value due to the uneven transport of potassium anions through the ion channels of the PAA chip. The whole sensing can be finished within 40 min, and there is no need for gene amplification. The CRISPR/dCas9–based sensor demonstrates ultrasensitive detection performance in the concentration range of 50 to 200 ng/μL and it has been proved to be feasible for the genome sequence of patient tissues. This sensor shows the potential of targeting other mutations by designing corresponding sgRNAs and expands the applications of CRISPR/dCas9 technology to the on-chip electrical detection of nucleic acids, which will be very valuable for rapid diagnosis of clinically mutated genes. This hybrid CRISPR-PAA chip makes it an ideal candidate for next-generation nucleic acid biosensors.

Introduction

Diffuse large B-cell lymphoma (DLBCL) shows significant heterogeneity in clinical features, gene expression, therapeutic response and prognosis. The need to detect MYD88^{L265P} mutation in clinical DLBCL samples is in great demand because this mutation is a crucial indicator for the rapid diagnosis and targeted treatment of DLBCL. The myeloid differentiation primary response 88 (MYD88) is an adaptor protein that interacts with receptors containing a Toll/interleukin-1 receptor (TIR) domain. MYD88 mutations constitutively activate NF-κB and its associated signaling pathways. There are many clinically significant mutations associated with DLBCL, including MYD88, CD79B, and BCL6, etc. High frequencies of the MYD88^{L265P} mutations are observed in DLBCL, demonstrating its potential as a prognostic and therapeutic biomarker directing precision medicine.[1, 2]

Single-nucleotide variant (SNV) is an important molecular marker for biomedical research and clinical application. Many clinical diseases are caused by single-nucleotide substitutions in genes.[3-5] Over the past 30 years, many methods have been established and optimised to detect targeted genomic sequences, such as quantitative polymerase chain reaction (qPCR), digital polymerase chain reaction (dPCR)[6, 7] and Sanger sequencing. [8-10] Although these tools for SNV have been proven to be effective, their applications in point-of-care tests are limited by complicated procedures and instruments, expensive reagents, trained operators, and high-level operation environments, etc. These reduce the accessibility of disease detections and limit their applications for real-time diagnosis and treatment of patients remotely. More importantly, these methods for quantitative analysis of nucleic acids usually require an amplification process, which requires a multi-step reaction and is more time-consuming.[11] Therefore, new strategies are needed to overcome these limitations to provide non-amplifying and high-efficiency nucleic acid diagnostic tools to cooperate with clinical treatment.

[a.] *Department of Biopharmacy, School of Pharmaceutical Sciences, Jilin University, 1266 Fujin Road, 130021 Changchun, China; orcid.org/0000-0002-6719-7579. Email: liang@jlu.edu.cn*
[b.] *Institute of Frontier Medical Science, Jilin University, 1163 Xinmin Street. 130021 Changchun, China; orcid.org/0000-0002-6280-2063. Email: sunfei@jlu.edu.cn*
[c.] *State Key Laboratory of Supramolecular Structure and Materials, Institute of Theoretical Chemistry, College of Chemistry, Jilin University, 2699 Qianjin Ave. 130012 Changchun, China; orcid.org/0000-0002-6216-6175; Email: xusp@jlu.edu.cn*
[d.] *Department of Hematology, The First Hospital of Jilin University, Jilin University, 71 Xinmin Street. 130021 Changchun, China; orcid.org/0000-0003-4066-9473; Email: baiou@jlu.edu.cn.*
†These authors contributed equally to this work.
Electronic Supplementary Information (ESI) available: material, primer and sgRNAs sequences (Table S1, Figure S1), binding reaction system (Table S2), X-ray photoelectron spec-troscopy (Figure S2), SDS-PAGE detection results correspond to dCas9 protein (Figure S3), the optical photograph of the PAA (Figure S4), schematic diagram of the passage about K^+ and Cl^- through PAA (Figure S5), screening results of KCl electrode buffer concentration (Figure S6),and Clinical information of 13 patients and corresponding MYD88^{L265P} detection results(Table S3, Figure S7).

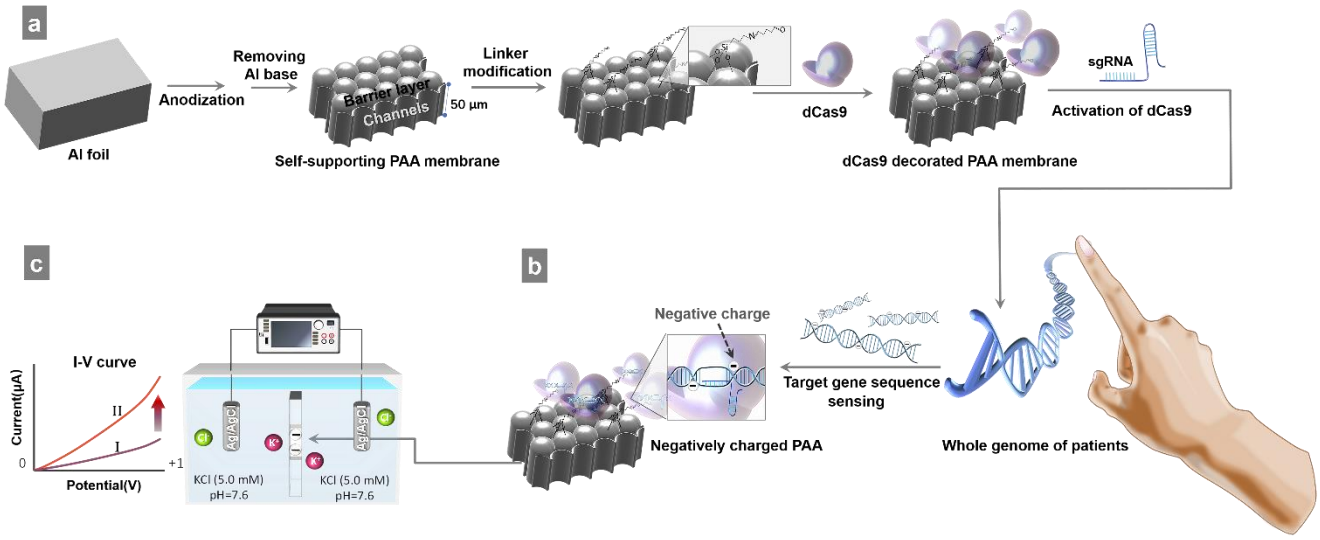

Fig. 1 Schematic illustration of the detection principle and detection procedure of the MYD88^{L265P}. (a) Surface modification procedures of PAA membrane. (b) The process of dCas9/gRNA complex binding to the patients' whole genome. (c) Electrochemical analyses for the whole genome DNA without amplification by the dCas9/gRNA decorated PAA chip.

While the wide-ranging applications and potential of clustered regularly interspaced short palindromic repeats (CRISPR)-associated nuclease (Cas) continue to expand, the CRISPR/Cas system has already been at work in many fields.[12, 13] Meanwhile, the CRISPR/Cas-based diagnostic applications have emerged and spread rapidly. The CRISPR-associated proteins, guided by a single-stranded RNA, are powerful tools for sequence-specific targeting and detections. The inactive Cas9 proteins (deactivated Cas9, dCas9) do not interfere with DNA hydrolysis, and they only bind to the specific DNA region without interrupting the target DNA. Thus, the CRISPR/dCas9 systems have been used to identify various pathogens in clinical samples, including viruses, tuberculosis, pertussis, malaria, and tumour mutants.[14, 15, 16] The CRISPR/dCas9 have yielded far more than just Cas9-based genome-editing tools,[17, 18] displaying the innovative impacts in liquid biopsy and diagnosis fields.[19] Van Donge et al., Mahfouz et al. and Li et al. discussed the developments and challenges of CRISPR/dCas9 systems in nucleic acid detections.[20-22] However, amplification techniques are still needed to improve sensitivity in these methods. In most developed CRISPR/Cas sensing strategies, a fluorescence turn-on mechanism based on the cleavage of a fluoresce-quencher pair by Cas proteins was employed. However, the detection signal of this method is not stable enough and is easily affected by environmental factors. More importantly, noise interference has a great influence on SNV detections. Aran et al. developed a non-amplification CRISPR system based on a graphene-based field-effect transistor.[23] This solid-supporting chip is an ideal candidate for next-generation nucleic acid biosensors.

Here, we develop a novel gene mutation detection strategy based on a CRISPR-dCas9 genome editing system, which can target specific sequences and directly detect the clinic samples (MYD88^{L265P} mutation of DLBCL) by an electrochemical ionic current rectification (ICR) technique without an amplification action. The specific primers for MYD88^{L265P} and its sgRNA were firstly screened and assessed. The sensing chip was constructed by immobilising the deactivated Cas9 (dCas9) proteins and the synthetic guide RNA (sgRNA) as the biorecognition receptor on the barrier layer surface of a porous anodic alumina (PAA) membrane (Fig. 1a). The CRISPR-PAA membrane spacing between two Ag/AgCl electrodes in an electrochemical cell can capture the target genes (Fig. 1b, c), which leads to the ICR changes of the PAA, since the fixed negatively charged genes will cause interference in K^+ ion transport.[24-26] The method is specifically available for targeting any 20 bp sequences. [27] This method can be a feasible SNV detection tool for other target genes in different scenes that require rapid response and simple preparation, and its amplification-free merit allows potential applications for field detections and point-of-care testings. Compared with traditional nucleic acid testing methods, including next-generation sequencing, isothermal amplification and qPCR, which are expensive and time-consuming, require bulky equipment, well-trained personnel, and specific testing environments, [28, 29] this biosensor afford the merits of rapidity, simplicity, and high selectivity.[28, 30]

Experimental

Recombinant Expression, Fermentation and Purification of dCas9 Protein

When the cleavage activity domains (RuvC and HNH) of the Cas9 protein are inactive, Cas9 (Genbank：LC477681.1) will keep its identification feature, but lose the nuclease cleavage activity, becoming a dCas9 protein. The expressed dCas9 protein belongs to S. Pyogenes (Spy). In this study, we explored not only

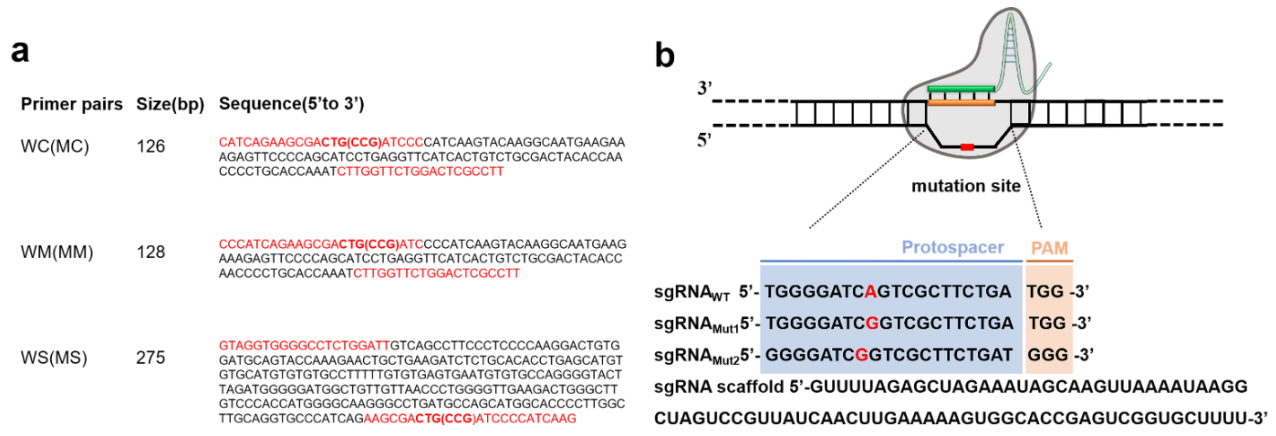

Fig. 2 (a) The PCR amplified gene fragment corresponding to the primers. (b) The relevant sequence information of sgRNAs was designed and screened.

the prokaryotic expression of dCas9 protein, but also the pilot fermentation process and the purification process of dCas9 protein. First, the expression vector of dCas9 was constructed, and pCold IV was selected as the expression vector. The *Escherichia coli* competent strain BL21 (DE3) strain containing the recombinant plasmid was cultured at37°C until OD_{600}=0.6, and the expression was induced by IPTG with a final concentration of 1.0 mM at different temperatures (16°C /25°C /37°C) for 8 h. Then, IPTG with the final concentrations of 0.1, 0.5, 1.0, and 2.0 mM were used to induce expression at 16℃ for 8 h. The supernatant and precipitates obtained from the bacterial liquid after high-pressure crushing was tested by odecyl sulfate, sodium salt-polyacrylamide gel electrophoresis (SDS-PAGE). The last step was to optimise the induction timing. The BL21 (DE3) strain containing the recombinant plasmid was cultured at 37℃ to OD_{600} at 0.4, 0.6, and 1.0, respectively, and then expressed at 16℃ with IPTG with a final concentration of 1.0 mM for 8 h (Fig. S3c in ESI). Next, the expression strain was fermented using a 7.5 L fermentor. Finally, the fermentation broth was purified using affinity chromatography, and the purity was verified by SDS-PAGE electrophoresis (Fig. S3d in ESI).

Design, Screening and Optimisation of sgRNA

The sgRNA is an important part of the CRISPR system, and the screening and optimisation of sgRNAs are essential for the stability of the system. Mutants often differ from wild-type samples by only one or a few bases, making it difficult to distinguish them by conventional testing techniques. Through the specific design of sgRNA, the site differences between the mutant and the wild-type samples could be accurately distinguished. For $MYD88^{L265P}$ sequence design of specific recognition sgRNA containing mutation sites and low off-target efficiency, the CCTop-CRISPR/Cas9 target online predictor, an online sgRNA design software (www.deskgen.com/landing/cloud), was used to screen genes in the conservative area can be targeted sites, determine the species and Cas9 protein recognition site. For DLBCL analysis via CRISPR–PAA, the sgRNAs were designed and validated to target $MYD88^{L265P}$. These sgRNA sequences were synthesised using HiScribe T7 High Yield RNA Synthesis Kit (NEB) following the Standard RNA Synthesis protocol. In summary, 1 μg of genomic DNA (gDNA) was incubated with 1× reaction buffer, 10 mM NTPs and T7 RNA polymerase enzyme mix at 37°C for 2 h followed by the DNase I treatment at 37°C for 15 min to remove gDNA from the reaction. sgRNA was then purified using RNA Clean & Concentrator Kits (Zymo Research). The sgRNA was diluted to 100 pmol/μL.The obtained sgRNA should be stored at -80°C to avoid degradation and contamination.

Three groups of primers with mutation sites (MC/MS/M) and three groups of primers without mutation sites (WC/WS/WM) were used for PCR amplification of the extracted whole genome sequence (Fig. 2a) to compare and screen the specific primers that work for screening specific positive patients initially. Through the early software design and experimental optimisation, several sgRNAs were preliminarily screened. PAM sequence, sgRNA scaffold, and sgRNAs that specifically bind to mutation sites were further identified, as presented in Fig. 2b.

qPCR Detection and Sanger Sequencing Method

The qPCR was performed on the Ct values from all DLBCL samples using the Analytic Jena Q-tower system (Analytik-Jena, Jena, Germany) with the 20 μL reaction system, including 5 μL complementary DNA product, 0.5 μL each primer (Table S1 in ESI), and 10 μL SYBR Green mix (Takara, Dalian, China). The PCR program was settled as one cycle of 10 min at 95°C followed by 45 cycles of 10 s at 95 °C, 30 s at 54 °C, and 30 s at 72 °C, and melting curve analysis was performed from 60 to 85°C with 0.1°C incremental increases. Quantification of DNA levels was based on the CT value and calculated with the $2^{-\Delta\Delta CT}$ method. Sanger sequencing is considered as the gold standard for detecting mutations of tumour samples. The extracted whole genome was firstly amplified by the PCR method to obtain a sequence of about 300 bp, which was purified and then sequenced by Sanger sequencing. The original sequence was compared to determine the presence of mutation sites.

PAA Chip Modification

The aluminium foil with 99.999% purity firstly experienced high-temperature annealing, mechanical polishing, ultrasonic and chemical treatment to remove lipid impurities and natural oxide layer on its surface. Then, the aluminium foil was calcined at

500 °C for 5 h in a vacuum condition. Next, it was placed into a mixed aqueous solution of concentrated sulfuric acid and phosphoric acid for electrochemical polishing. After that, the treated aluminium foil was anodised in two steps at room temperature to obtain a porous anodised alumina film. The specific surface modification steps of PAA are as follows. (1) The PAA was first ultrasonic cleaned with pure water for 2 min and then dried with nitrogen. (2) Hydroxylation treatment: we applied a corona gun external flame to burn the blocking layer repeatedly and make it hydroxylated evenly. (3) Amino treatment: After the hydroxylated treatment, the barrier layer was exposed to a 3-aminopropyltriethoxysilane (APTES) solution (2%) and treated overnight to make it fully activated. After that, the PAA membrane surface was washed with a large amount of ethanol and dried with nitrogen. After they were cleaned with pure water several times and dried with nitrogen, the PAA membranes were heated at 120 °C for 1 h to make the molecules dehydrated and cross-linked. (4) GA assembly: The surface of the barrier layer was immersed in a 10% GA solution (glutaraldehyde solution was prepared with PBS buffer) and reacted at 4 °C for 4 h to connect the aldehyde group. Then, the PAA with aldehyde modification was rinsed and dried with water. (5) Assembly of dCas9 protein on PAA surface: The protein solution was dropped on the surface of the barrier layer and reacted overnight at 4 °C. Then the membranes were rinsed with a PBS buffer for later use.

Biosensing Performance

After incubation with dCas9 protein, the PAA was washed with pure water and dried under a gentle nitrogen stream. Then 0.5 µL of 100 pmol/µL of sgRNA was dropped on PAA and incubated for 20 min at 37 °C, and the environment was kept as humidity to prevent evaporation of the dropped solution. Next, the PAA was washed with pure water dried with nitrogen. Then, 10 µL of gDNA was dropped on PAA and incubated for 20 min in 37°C. Finally, the immobilised dCas9 is complexed with an sgRNA, specific to a gDNA target, forming the dCas9/sgRNA complex. The whole genome was diluted as a mass gradient of 0, 250, 500, 1000, 1500, 2000 and 2500 ng. The modified PAA membrane was fixed to the electrochemical detection device (Fig. 1c) for current-voltage scanning detection. Previous experiments have verified that electrolyte concentration can affect the current-voltage (I–V) relation. A KCl buffer was added to a glass tank connecting to the Ag/AgCl electrode. The voltage was adjusted from 0 to 1 V, and the current was set as 0.5 A. We first scan the current-voltage relations of different concentrations of KCl, and found that 5.0 mM of KCl (pH =7.6) solution as the electrolyte is more proper in the present study. This concentration was selected for a series of subsequent patch-modification and electrochemical tests of the patients' entire genome sequence. The current changes of bare PAA, hydroxylation, APTES, aldehyde modification, and the combination of dCas9 and sgRNA, were recorded. The parallel groups were set and the current values at 1 V were plotted. At least three trials were recorded to calculate the standard deviation of each sample. Standard curves and current changes were obtained for positive samples.

Patient Selections and Sample Collection

DLBCL patients, who have been newly diagnosed without being treated with any drug or surgical operations, were chosen for this study. A total of 13 patients suspected of DLBCL surgery admitted to the Hematology Department of Tumor Center of the First Hospital of Jilin University were collected. Involved subjects have been signed the informed consent, and this study was reviewed by the Medical Ethics Committee of the First Hospital of Jilin University (project batch number: 2021-451). More information about the patient samples is listed in Table S3 in ESI. Tissue samples were collected in sterile tubes containing tissue preservation solution and stored in liquid nitrogen until use. Blood/Cell/Tissue Genomic DNA Extraction Kit from TIANGEN® was used, which extracted the whole genome of tissue samples. High purity gDNA can be obtained within 1 h using the kit. These contained one control assay and three mutations assays to be run in a qPCR assay. At the same time, the comparison of Sanger sequencing results shows the advantages of our research method. All consumable plastic or glass equipment was obtained as Dnase-free, Rnase-free and sterile types.

Results and discussion

Identification of MYD88^{L265P} Specificity and Verification of sgRNA Activity

The screening of the Locus-specific primers for MYD88^{L265P} was firstly carried out, and the validation of sgRNA activity was tested by the electrophoresis approach. Multiple groups of primers were used for the comparison and screening of positive samples M1 and M2, and the electrophoresis results are shown in Fig. S1a in ESI. MS primer pairs with mutated sites corresponding to lane 5 and lane 10 show better specificity than other primer pairs. Table S1 in ESI lists the primer sequences. Three groups of primers with mutation sites (MC/MS/M) and three groups of primers without mutation sites (WC/WS/WM) were used for the PCR amplification of the extracted whole genome sequence (Fig. 2a), to compare and screen the specific primers that work for screening specific positive patients initially. Primer pairs are labelled with red, and mutation sites are treated with bold on the basis of red, and the mutant bases are in parentheses. The positive sample M3 was also verified by the same method, as shown in Fig. S1b in ESI. According to the electrophoresis results, MS primer pairs with mutated sites corresponding to lane 3 exhibit better specificity than other primer pairs. MS primer pairs also have better detection specificity than the wild-type primer pairs. Thus, they were chosen for further CRISPR-PAA and qPCR assays.

The activity of sgRNA is the basis of the CRISPR/dCas9 technology and the key to the specificity of the CRISPR/dCas9-based sensing method. It is necessary to verify the activity of sgRNA that can specifically bind to sequences containing MYD88^{L265P}. This method can conduct a preliminary screening of multiple sgRNA and determine mutant samples. The electrophoresis results of three positive patients with MYD88^{L265P} (M1/M2/M3) were observed in Fig. S1c-e in ESI. The

binding reaction system was configured according to Table S2 in ESI. The MS primer pairs were used in the electrophoresis experiment to verify their binding activity. According to the electrophoretic results (Fig. S1 in ESI), the binding efficiency of 0.5 µL of sgRNA with the concentration of 100 pmol/µL in 20 µL system is higher than 1.0 µL. Among them, lane 1 and 2 in Fig. S1d in ESI represent the original sample amplified by the MS primer pairs. They have little difference in size and trend compared to band 2 that has no dCas9 protein. The presence of double bands in Fig. S1e in ESI can be explained by the partial degradation of the amplified sequence during the electrophoretic operation, which has no effect on the binding reaction theoretically. It can be seen from Fig. S1 in ESI that the binding effect in the reaction system is relatively apparent compared with the original sample. Through the early simulation and experimental optimisation, several sgRNAs were preliminarily screened. PAM sequence, sgRNA scaffold, and sgRNAs that specifically bind to mutation sites were further identified (Fig. S1b in ESI). After preliminary screening, sgRNA with a sequence as 5'UGGGGAUCGGUCGCUUCUGAGUUUUAG AGCUAGAAAUAGCAAGUUAAAAUAGUCGCUUCUGAAGGCUAG UCCGUUAUCAACUUGAAAAAGUGGCACCGAGUCGGUGCUUUU 3', was chosen to target the gDNA sequence of MYD88^{L265P}.

MYD88^{L265P} Detection Using the qPCR and Sanger Sequencing Methods

A variety of strategies can be used to assess MYD88^{L265P} status in tumour samples, including Sanger sequencing, qPCR with melting curve analysis (MC), and pyrosequencing (PS). We used qPCR and Sanger sequencing to screen and verify the mutant sites at MYD88^{L265P}, in comparison to our developed electrochemical method. The qPCR was performed on the Ct values from all DLBCL samples using the Analytic Jena Q-tower system (Analytik-Jena, Jena, Germany) with the 20 µL reaction system. Quantification of DNA levels was based on the Ct value and calculated with the $2^{-\Delta\Delta CT}$ method. The wild-type sequences were extracted from the whole genome. Three positive sequences with MYD88^{L265P} mutation were firstly amplified by PCR with universal primers (Table S1 in ESI), and then purified and sent to a sequencing company for Sanger sequencing. The original sequence was compared to determine the presence of mutation sites. The sequencing results of wild-type and three mutant sequences are shown in Fig. 3a. Compared with the wild-type sequencing results (panel ⅰ), the mutant groups show significant base mutations (panel ⅱ, ⅲ and ⅳ) (CTG-CCG), precisely evidencing the presence of MYD88^{L265P}.

The qPCR results corresponding to the wild type and three groups of positive mutation sequences are shown in Fig. 3b. MS primers were used to configure the qPCR system. Compared with the control group, the relative expressions of the three mutant groups are much higher, indicating that mutation genes can be clearly identified in positive patient samples.

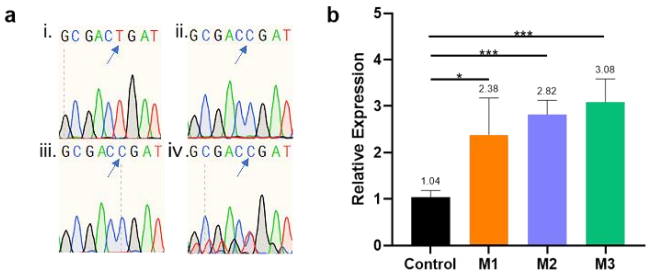

Fig.3 Schematic diagram of sanger sequencing and qPCR detection results. (a) Sequencing results of the wild-type (ⅰ), sequencing results of M1 (ⅱ), sequencing results of M2 (ⅲ), sequencing results of M3 (ⅳ). The arrows point to the mutation site. (b) The qPCR results of wild type and three mutant sequences. Significance was determined by the unpaired t-test. (*P < 0.05; **P < 0.01; ****P < 0.0001).

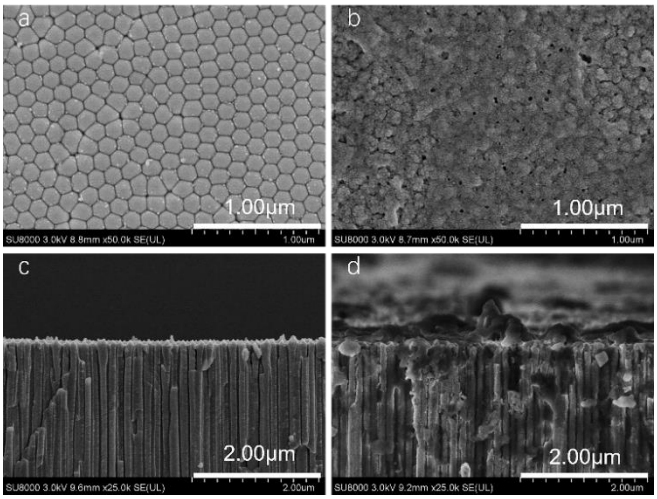

Fig.4 SEM images of the as-prepared PAA-based sensing membrane. (a) Top view of a blank chip. (b) Top view of a chip modified with the dCas9 protein. (c) The cross-section of a blank chip. (d) The cross-section of a chip modified with the dCas9 protein.

Surface Modification Identification of CRISPR–PAA Chip

Many analytical techniques have been combined with CRISPR/Cas systems for DNA/RNA detections, for instance, fluorescence,[30] liquid-gated graphene field-effect transistors [23], and surface-enhanced Raman scattering (SERS).[31] Here, we developed a CRISPR-mediated electrochemical detection platform based on the ion-channel feature of the PAA membrane.

PAA with hexagonal close-packed arrangement has a broad application prospect because of its simple preparation method, low cost, solid structure and stable physical and chemical properties.[32] PAA with a high aspect ratio, orderly and controllable size, high hardness, high-temperature resistance can be used as a good solid-supporting template not only for the

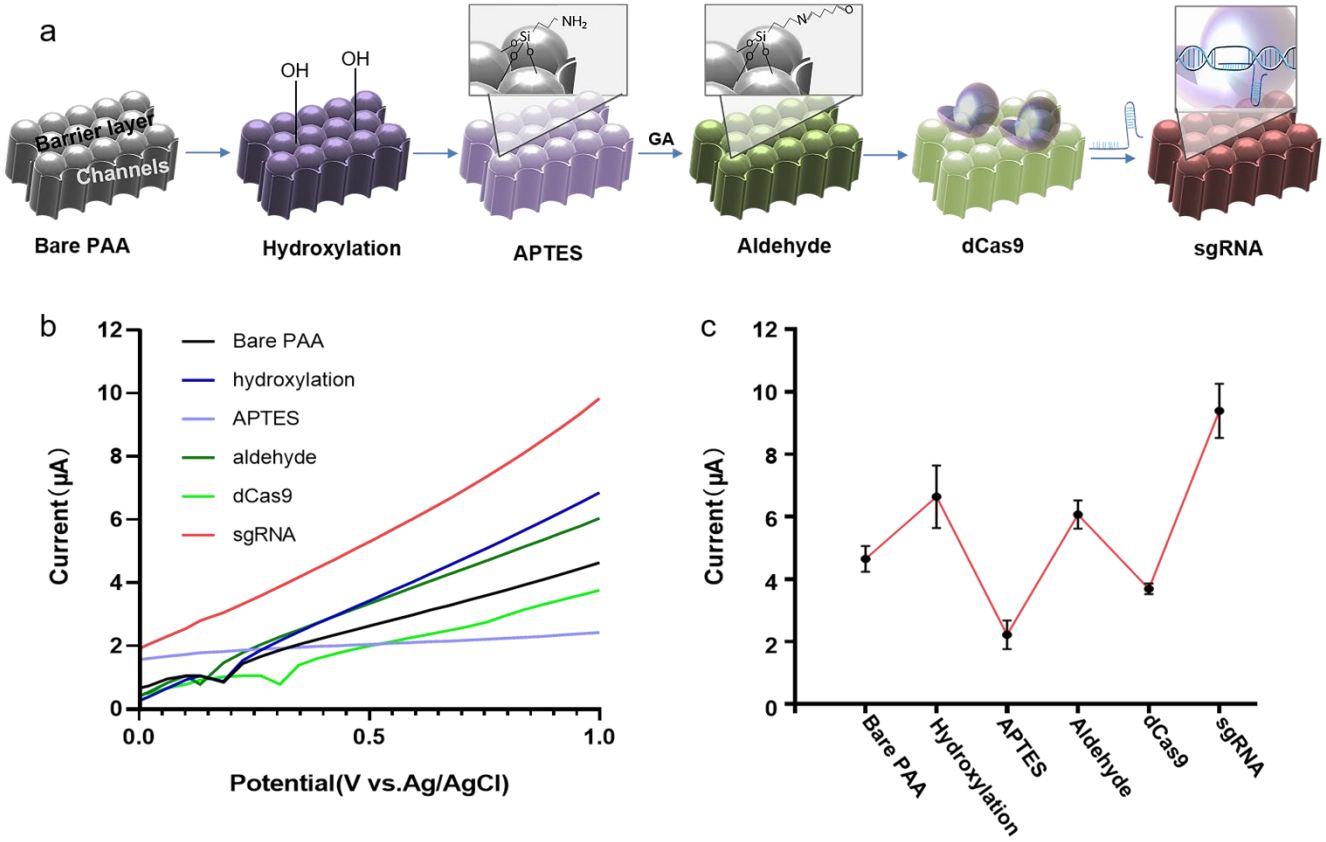

Fig.5 (a) Schematic diagram of PAA chip modification process. (b) The I–V curves of the pure hybrid PAA before and after surface modifications. (c) Detection charts of three parallel groups were set for each modificatory step. The current values at 1 V of the PAA membrane before and after the surface was modified with hydroxylation, APTMS, aldehyde, dCas9, and sgRNA, respectively.

growth of nanometer materials inside, but also for the surface decoration on the inner surfaces or the barrier surfaces. It has been reported that the surface-modified PAA could play as nanochannel and ion-channel hybrid electrochemical sensors according to the steric blockage and charge repulsion.[33-36] Inspired by these publications, we combined the ion-channel PAA with the CRISPR/dCas9 protein to develop a novel CRISPR-mediated electrochemical detection platform. The PAA membrane we used in the present study is a self-supporting PAA (~50 μm in thickness) with the removal of Al base, and the barrier layer side is the location where the CRISPR/dCas9 proteins are anchored. The PAA was prepared by a two-step oxidisation method, and its scanning electron microscopic (SEM) images (Fig. 4a,c) show that PAA has straight channels with a size of about 18 nm. The barrier layer surface of the PAA chip experienced hydroxylation, amination and was further modified with aldehyde to stably bind the dCas9 protein (as presented in Fig. 1a), verified by X-ray photoelectron spectroscopy (Fig. S2 in ESI).

The dCas9 proteins were obtained from *Escherichia coli* BL21 in our laboratory. The expression vector was successfully constructed. The molecular weight of the dCas9 protein is known to be 159 kD. By setting different conditions and verification through SDS-PAGE, the optimal induction expression conditions of dCas9 protein were found as: IPTG concentration of 1.0 mM, induction temperature of 16 ℃, and induction when OD600=0.6 (Fig. S3 in ESI). After dCas9 protein modification, the top view (Fig. 4b) and cross-section (Fig. 4d) show that the PAA membrane becomes rough, demonstrating that the dCas9 proteins have been fixed on the PAA membrane. The effective sensing area is a disc with 0.5 mm in diameter (Fig. S4 in ESI).

The sensing mechanism of this CRISPR-mediated electrochemical detection platform is based on a phenomenon found throughout natural ion channels where asymmetric ionic currents respond to bias voltage in different directions. The electric double layer (EDL) theory is essential to explain the ionic flux. The asymmetric ion current response is caused by the regulation of the directional movement of cation and cation by the double-layer structure in the inner wall of the channel at the nanoscale, which is traceable by the electrochemical voltammetry curves.[37] When the bias voltage is applied between two electrodes, the cation and anion in the electrolyte solution migrate inside and outside the channel, and the ionic current is generated (Fig. S5 in ESI). In our case, two Ag-AgCl electrodes were put on two sides of the PAA membrane with a

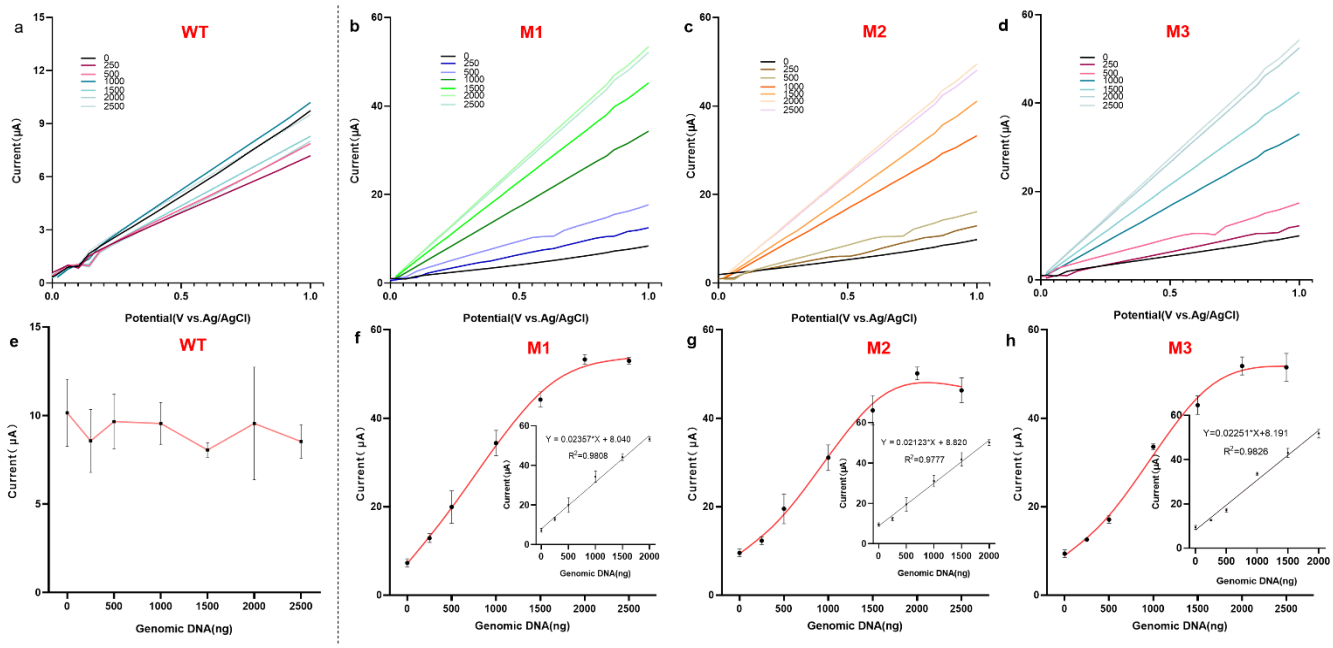

Fig.6 The sensitivity and selectivity of the CRISPR–PAA sensing chip for MYD88^{L265P} contained within whole genomic DNA samples. (a) Schematic diagram of the change of current value as the sample mass of WT (Wild type) is added. (b) Schematic diagram of the change of current value as the sample mass of M1 (Mutant1) is added. (c) and (d) correspond to the schematic diagram of M2(Mutant2) and M3(Mutant3) sample current value changes, respectively. (e) The intensity curves of the parallel samples of W(Wild), under the condition of +1.0 V. (f), (g), (h) The intensity curves of the parallel samples of M1, M2, and M3, respectively, under the condition of +1.0 V. And CRISPR–PAA sensitivity calibration curves according to the genomic DNA with MYD88^{L265P}.

distance of about 3.0 cm. An electrochemistry workstation was used to set the detection parameters, and the current-voltage detection curves were obtained. The electrolyte is the 5.0 mM KCl solution with pH =7.6 (see Fig. S6 in ESI). The unmodified PAA has an iso-electric point size of 6.5. [38] It will be negatively charged in a pH = 7.6 buffer. So, it attracts the positively charged potassium ions (K^+) and repels the negatively charged chloride ions (Cl^-) when ions are driven by an electric field. The phenomena of K^+ and Cl^- passing through PAA at different voltage ranges are different (Fig. S5 in ESI). The voltage was scanned from 0~1.0 V, with the scanning rate of 0.05 V/s, and the corresponding curves were recorded. Finally, we used the ionic current recorded at +1 V to reflect the concentration of the gene to be tested. Electrochemical detections were carried out after each modification step, including bare PAA, hydroxylation, 3-aminopropyltriethoxysilane (APTES), aldehyde modification, and the combination of dCas9 and sgRNA (Fig. 5). Bare PAA has negatively charged at a 5.0 mM KCl solution with pH = 7.6 buffer. Its current is stable at about 3 μA. The increase of positive charge after hydroxylation and aldehyde led to an upward trend of the current value. After the APTES modification, the mean current value alters to 2.229μA due to the positive charges of APTES. And the current value is obviously reduced, indicating that the modification effect is excellent. The iso-electric point of the dCas9 protein is 9.01, showing an average current of 3.691μA. After the combination of sgRNA, the chip shows a negative state, leading to the current increase (Fig. 5), proving the successful assembly of dCas9 proteins.

Clinical Utility of CRISPR–PAA Sensing Chip for Detection of MYD88^{L265P} Mutations

The developed CRISPR–PAA device was employed to directly test the MYD88^{L265P} mutation genes of clinic patient genomic DNA samples without amplification or purification. [31] Genome-wide DNA was derived from tissue removed after surgery in patients with lymphoma.

The step that sgRNA specifically identifies MYD88^{L265P} activated dCas9 protein took 20 min. Next, the dCas9/gRNA complexes on the PAA chip were exposed to the genomic DNA from patients with DLBCL (Fig. 1b) for an incubation time of about 20 min. Because dCas9/gRNA can capture the complementary target DNA by identifying the specific site, the dCas9/gRNA complexes can accurately bind with the MYD88L265P gene.

We further traced the mass gradients of three positive mutation samples (M1/M2/M3) by our developed CRISPR-PAA biosensors, and the voltage-current curves are shown in Fig. 6b-d. The increase was significant compared to wild-type patients without the mutation (WT) (see Fig. 6a,e). The concentration gradient detections of clinical genetic samples were first obtained. According to the genomic DNA mass gradient, a calibration curve was made to assess linearity and reproducibility. Three parallel tests were set for each quality point to verify the accuracy of the data and the stability of the trend. A good linear relationship is observed between 0 and 2000 ng. Reproducibility was tested by calibration curves and assessing the regression coefficient (R^2=0.9826/0.9808/0.9777), indicating our sensing method has good relevance and credibility. Meanwhile, the intensity curve of the parallel

samples corresponding to the tested standard curve at +1.0 V is shown. It can be seen that the significant increases in current values are found in a range of 0-2000 ng (Fig. 6f-h). Clinical sample assays are in agreement with qPCR and Sanger sequencing method results. The recorded curves from the CRISPR–PAA sensing chip for the other 9 clinical patient samples are displayed in Fig. S7 in ESI. We can see that except for the three positive mutation patients, all the other patients showed a negative state. The accuracy of the detection was also confirmed according to the later NGS results. Specific sgRNA is designed for accurate detection of SNV, so that we can clearly distinguish between different clinical samples and avoid false positives.

The limits of detection (LODs) of the CRISPR–PAA system were assessed according to the molecular weight achieved by PCR amplification with universal primers, and the calculated LOD is 1.37 nM according to the added mass of 1000 ng. The trend of the current increase proves to be linear with expectations. It should be noted that only 500 ng of the genomic clinical sample was tested for each trial in this method. If considering the molecular weight of the human genome (1.9×10^{12} g/mol)[40], the detection sensitivity of the present method can reach the fM level, which is comparable to previous study[39] in which they reported a genomic detection of unamplified clinical samples with a sensitivity of 1.7 fM.

Conclusions

Aiming at the SNV detection of $MYD88^{L265P}$ of DLBCL without gene amplification, we screened a sensitive sgRNA sequence for the CRISPR/dCas9 identification system. Further, we developed a label-free CRISPR/dCas9 assay based on an ion-channel-based electrochemical detection method, with the advantages of speed, sensitivity, and site-specific detection ability for different mutation genes according to the ICR effect. This electrochemical CRISPR/dCas9-based assay is available for 20 bp sequence detections and can be feasibly extended for other nucleic acid detection systems only by changing other target-matching sequences. In view of the growing demand for portable devices for molecular diagnostics, future versions of CRISPR-PAA might offer an easy-to-handle, versatile and rapid on-chip solution for genome-based diagnostics. The possible application of the technique with other important mutations in a stable and efficient system may be a promising area in the early diagnosis of cancers and promoting the development of biosensors one step forward toward robust point-of-care systems and clinically applicable genotype screenings. Particularly it is necessary to face life-threatening situations where a timely diagnosis can make a precise treatment.

Author Contributions

Dr. C. L., Prof. F. S., and W. S.: investigation, validation, writing, original draft, visualisation. W. S., Z. L., S. Q., and Z. W.: Conceptualisation, formal analysis, visualisation, Investigation. L. Q., and L. S.: investigation, validation. W. G. and Prof. O. B.: contributed valuable clinical samples and ethical data. Dr. C. L., and Prof. S. X.: conceptualisation, methodology, supervision, writing, review & editing, project administration, funding acquisition, resources.

Conflicts of interest

There are no conflicts to declare.

Acknowledgements

The authors acknowledge the staff of the Institute of the Frontier Medical Science for the experimental support and Shulin Guan, Jilin Univ. for her helpful discussion about PAA. This study was financially supported by the Science and Technology Project Foundation of Jilin Province (No.20190304035YY) and Interdisciplinary Integration Innovation Project of Jilin University (JLUXKJC2020106).

References

1 V. N. Ngo, R. M. Young, R. Schmitz, S. Jhavar, W. Xiao, K.-H. Lim, H. Kohlhammer, W. Xu, Y. Yang, H. Zhao, A. L. Shaffer, P. Romesser, G. Wright, J. Powell, A. Rosenwald, H. K. Muller-Hermelink, G. Ott, R. D. Gascoyne, J. M. Connors, L. M. Rimsza, E. Campo, E. S. Jaffe, J. Delabie, E. B. Smeland, R. I. Fisher, R. M. Braziel, R. R. Tubbs, J. R. Cook, D. D. Weisenburger, W. C. Chan and L. M. Staudt, *Nature*, 2010, **470**, 115–119.
2 C. Visco, I. Tanasi, F. M. Quaglia, I. Ferrarini, C. Fraenza and M. Krampera, *Cancers (Basel)*, 2020, **12**. (10).
3 Q. Xu, S. Q. Huang, F. Ma, B. Tang and C. Y. Zhang, *Anal. Chem*., 2016, **88**, 2431–2439.
4 G. D. Poznik, Y. Xue, F. L. Mendez, et al., *Nat. Genet*., 2016, **48**, 593–599.
5 E. Khurana, Y. Fu, D. Chakravarty, F. Demichelis, M. A. Rubin and M. Gerstein, *Nat. Rev. Genet.*, 2016, **17**, 93–108.
6 V. Taly, D. Pekin, L. Benhaim, S. K. Kotsopoulos, D. Le Corre, X. Li, I. Atochin, D. R. Link, A. D. Griffiths, K. Pallier, H. Blons, O. Bouche, B. Landi, J. B. Hutchison and P. Laurent-Puig, *Clin. Chem*., 2013, **59**, 1722–1731.
7 E. A. Ottesen, J. W. Hong, S. R. Quake and J. R. Leadbetter, *Science*, 2006, **314**, 1464–1467.
8 L. Cao, X. Cui, J. Hu, Z. Li, J. R. Choi, Q. Yang, M. Lin, L. Ying Hui and F. Xu, *Biosens. Bioelectron.*, 2017, **90**, 459–474.
9 P. L. White, C. Mengoli, S. Bretagne, M. Cuenca-Estrella, N. Finnstrom, L. Klingspor, W. J. Melchers, E. McCulloch, R. A. Barnes, J. P. Donnelly, J. Loeffler and P. C. R. I. European Aspergillus, *J. Clin. Microbiol.*, 2011, **49**, 3842–3848.
10 A. C. Tsiatis, A. Norris-Kirby, R. G. Rich, M. J. Hafez, C. D. Gocke, J. R. Eshleman and K. M. Murphy, *J. Mol. Diagn.*, 2010, **12**, 425–432.
11 I. Furlan, I. Domljanovic, J. Uhd and K. Astakhova, *Chembiochem.*, 2019, **20**, 587–594.
12 R. Barrangou, C. Fremaux, H. Deveau, M. Richards, P. Boyaval, S. Moineau, D. A. Romero and P. Horvath, *Science*, 2007, **315**, 1709–1712.
13 K. E. Uyhazi and J. Bennett, *J. Clin. Invest.*, 2021, **131**, e145214.
14 A. Maxmen, *Nature*, 2019, **566**, 437.
15 M. P. Hirakawa, R. Krishnakumar, J. A. Timlin, J. P. Carney and K. S. Butler, *Bioscience. Rep.*, 2020, **40**, BSR20200127.
16 A. Ramachandran, D. A. Huyke, E. Sharma, M. K. Sahoo, C. Huang, N. Banaei, B. A. Pinsky and J. G. Santiago, *Proc. Natl. Acad. Sci. U S A.*, 2020, **117**, 29518–29525.

17 E. V. Koonin, K. S. Makarova and F. Zhang, *Curr. Opin. Microbiol.*, 2017, **37**, 67–78.
18 A. Varble and L. A. Marraffini, *Trends Genet.*, 2019, **35**, 446–456.
19 S. E. Klompe and S. H. Sternberg, *Crispr. J.*, 2018, **1**, 141–158.
20 J. E. van Dongen, J. T. W. Berendsen, R. D. M. Steenbergen, R. M. F. Wolthuis, J. C. T. Eijkel and L. I. Segerink, *Biosens. Bioelectron.*, 2020, **166** :112445.
21 R. Aman, A. Mahas and M. Mahfouz, *Acs. Synth. Biol.*, 2020, **9**, 1226–1233.
22 M. Wang, R. Zhang and J. M. Li, *Biosens. Bioelectron.*, 2020, **165**, 112430.
23 R. Hajian, S. Balderston, T. Tran, T. deBoer, J. Etienne, M. Sandhu, N. A. Wauford, J. Y. Chung, J. Nokes, M. Athaiya, J. Paredes, R. Peytavi, B. Goldsmith, N. Murthy, I. M. Conboy and K. Aran, *Nat. Biomed. Eng.*, 2019, **3**, 427–437.
24 Y. Lin, Q. Lin, X. Liu, Y. Gao, J. He, W. Wang and Z. Fan, *Nanoscale Res. Lett.*, 2015, **10**, 495.
25 J. S. Park, D. Moon, J. S. Kim and J. S. Lee, *J. Biomed. Nanotechnol.*, 2016, **12**, 575–580.
26 C. Zhao, Y. Zhu, L. Chen, S. Zhou, Y. Su, X. Ji, A. Chen, X. Gui, Z. Tang and Z. Liu, *Nanoscale*, 2018, **10**, 16278–16283.
27 H. Z. Abid, E. Young, J. McCaffrey, K. Raseley, D. Varapula, H. Y. Wang, D. Piazza, J. Mell and M. Xiao, *Nucleic Acids Res.*, 2021, 49(2), e8.
28 R. Bruch, G. A. Urban and C. Dincer, *Nat. Biomed. Eng.*, 2019, **3**, 419–420.
29 C. Dincer, R. Bruch, E. Costa-Rama, M. T. Fernandez-Abedul, A. Merkoci, A. Manz, G. A. Urban and F. Guder, *Adv. Mater.*, 2019, **31**, e1806739.
30 Y. Li, S. Y. Li, J. Wang and G. Liu, *Trends Biotechnol.*, 2019, **37**, 730–743.
31 H. Kim, S. Lee, H. W. Seo, B. Kang, J. Moon, K. G. Lee, D. Yong, H. Kang, J. Jung, E. K. Lim, J. Jeong, H. G. Park, C. M. Ryu and T. Kang, *ACS Nano*, 2020, 14, 17241–17253.
32 J. M. Moon, D. Akin, Y. Xuan, P. D. Ye, P. Guo and R. Bashir, *Biomed. Microdevices*, 2009, **11**, 135–142.
33 R. Mo, L. He, C. Zhou, Z. J. Qian, P. Hong, S. Sun, Z. Wang, Y. Wang and C. Li, *Anal. Chem.*, 2019, **91**, 8184–8191.
34 H. Gao, R. Sun, L. He, Z. J. Qian, C. Zhou, P. Hong, S. Sun, R. Mo and C. Li, *ACS. Appl. Mater. Inter.*, 2020, **12**, 4849–4858.
35 S. J. Li, J. Li, K. Wang, C. Wang, J. J. Xu, H. Y. Chen, X. H. Xia and Q. Huo, *ACS Nano*, 2010, **4**, 6417–6424.
36 X. P. Zhao, F. F. Liu, W. C. Hu, M. R. Younis, C. Wang and X. H. Xia, *Anal. Chem.,* 2019, **91**, 3582–3589.
37 J. Cao, X. P. Zhao, M. R. Younis, Z. Q. Li, X. H. Xia and C. Wang, *Anal. Chem.,* 2017, **89**, 10957–10964.
38 C. Wang, X. P. Zhao, F. F. Liu, Y. Chen, X. H. Xia and J. Li, *Nano Lett.*, 2020, **20**, 1846–1854.
39 R. Hajian, S. Balderston, T. Tran, T. DeBoer, J. Etienne, M. Sandhu, N. A. Wauford, J. Y. Chung, J. Nokes, M. Athaiya, J. Paredes, R. Peytavi, B. Goldsmith, N. Murthy, I. M. Conboy and K. Aran, *Nature Biomedical Engineering.*, 2019, **3**, 427–437.
40 C. International Human Genome Sequencing, *Nature*, 2004, **431**, 931–945.